

BEHAVIORAL CHARACTERISTICS AND CO+CO₂ PRODUCTION RATES OF HALLEY-TYPE COMETS OBSERVED BY *NEOWISE*

J. D. ROSSER,^{1,2} J. M. BAUER,^{2,3,4} A. K. MAINZER,² E. KRAMER,² J. R. MASIERO,² C. R. NUGENT,³ S. SONNETT,²
Y. R. FERNÁNDEZ,⁵ K. RUECKER,³ P. KRINGS,³ AND E. L. WRIGHT⁶
THE *WISE* AND *NEOWISE* TEAMS

¹University of Rochester 206 Bausch & Lomb Hall P.O. Box 270171 Rochester, NY 14627-0171, USA

²Jet Propulsion Laboratory, California Institute of Technology, 4800 Oak Grove Drive, MS 183-401, Pasadena, CA 91109, USA

³Infrared Processing and Analysis Center, California Institute of Technology, Pasadena, CA 91109, USA

⁴Dept. of Astronomy, University of Maryland, College Park, MD 20742, USA

⁵Dept. of Physics, Univ. of Central Florida, 4000 Central Florida Blvd., Orlando FL 32816-2385, USA

⁶Department of Physics and Astronomy, University of California, Los Angeles, CA 90095, USA

(Received October 1, 2017; Revised January 30, 2018; Accepted February 19, 2018)

ABSTRACT

From the entire dataset of comets observed by *NEOWISE*, we have analyzed 11 different Halley-Type Comets (HTCs) for dust production rates, CO+CO₂ production rates, and nucleus sizes. Incorporating HTCs from previous studies and multiple comet visits we have a total of 21 stacked visits, 13 of which are active and 8 for which we calculated upper limits of production. We determined the nucleus sizes of 27P, P/2006 HR30, P/2012 NJ, and C/2016 S1. Furthermore, we analyzed the relationships between dust production and heliocentric distance, and gas production and heliocentric distance. We concluded that for this population of HTCs, ranging in heliocentric distance from 1.21 AU to 2.66 AU, there was no significant correlation between dust production and heliocentric distance, nor gas production and heliocentric distance.

Keywords: comets: general - infrared: planetary systems

1. INTRODUCTION

Comets are an accessible population of solar system bodies that manifest substantial volatile reservoirs which represent the primordial chemistry of the solar system. Comets are either brief visitors or relative newcomers to the inner solar system and so have spent most of their existence in the deep freeze of the outer solar system, where volatiles are relatively undepleted. It is generally inferred that the combined populations that constitute comet reservoirs, for example the Oort Cloud and Kuiper Belt Object populations, are more numerous than the other small body populations for the sizes of a few kilometers (cf. [Dones et al. 2015](#), [Bauer et al. 2017](#)). Cometary nuclei are defined as a combination of refractory and volatile materials, however, cometary populations differ by some of the most basic compositional, dynamical, and physical properties, indicating some evolution must take place. Mass loss (cf. [Jewitt 2014](#)), and selective depletion of specific volatile species like CO ([Meech & Svoren 2004](#); [Mumma et al. 2012](#); [A'Hearn & Dixi Science Team 2011](#)), are manifestations of these evolutionary effects. Ensemble properties of populations also show evidence of evolution ([Fernández et al. 2013](#); [Meech et al. 2004](#); [Bauer et al. 2017](#)) which may affect intermediary ([Bauer et al. 2013](#)) or end states ([Licandro et al. 2016](#)). Nonetheless, the prevalence of particular volatiles, such as CO and CO₂, may be more common among particular dynamical populations, e.g. long-period comets (LPCs) ([Ootsubo et al. 2010](#); [Reach et al. 2013](#)). It should be noted, however, that such volatiles are not universally present in detectable quantities for all LPCs. Hence, a component of compositional variation as well as evolutionary effects must be present in the cometary sub-populations. One possible way of discerning how strong compositional variations of particular species, such as CO and CO₂, are among LPCs is to study a population that is an evolutionary intermediary to the ultimate demise of the populations' members. Such an intermediary state for the LPCs are the Halley-type comets (HTCs), a subset of short period comets with orbital periods ranging from 20 yrs. to 200 yrs. HTCs have been shown to evolve primarily from LPC reservoirs ([Wiegert & Tremaine 1999](#)), hence, if HTCs and LPCs share similar origins, both evolving from Oort Cloud populations, HTCs may be used to determine the effects of insolation on LPCs, separate from original composition.

Various studies on organics for certain HTCs, e.g. by [Bönnhardt et al. \(2008\)](#) have been completed in the past. However, no previous study has presented a uniform survey of CO+CO₂ production for multiple HTCs. This is due primarily to the rarity of space-based platforms that

are capable of detecting CO₂. Such platforms also detect CO more easily than ground-based telescopes, since they are unencumbered by the Earth's atmospheric absorption. Observations of HTCs at large Earth-Sun distances is still relatively rare, thus these are some of the first in-depth analyses of CO and CO₂ production by such objects.

On 2009 December 14, the *Wide-field Infrared Survey Explorer* (*WISE*) was launched to complete a mid-infrared survey of the entire sky at 3.4, 4.6, 12, and 22 μm . These bands are respectively referred to as the W1, W2, W3, and W4 bands ([Wright et al. 2010](#)). The primary cryogen tank was fully exhausted by 2010 August 5, making the W4 band inoperable: this initiated the 3-Band phase (W1, W2, and W3 bands) of the mission until the secondary cryogen tank was depleted on 2010 October 1 ([Bauer et al. 2015](#); [Mainzer et al. 2011a](#)). After October 1, only the W1 and W2 bands remained operative. The mission then entered the four month *NEOWISE* Post-Cryogenic Phase with the purpose of finding minor planets, until 2011 February when the telescope went into hibernation ([Mainzer et al. 2011a, 2012](#); [Masiero et al. 2012](#)). On 2013 October 3, the *WISE* spacecraft was brought out of hibernation for the purpose of discovering and characterizing Near Earth Objects (NEOs) and other small bodies. The survey was restarted on December 13th, 2013, and the *NEOWISE* mission has been ongoing ever since ([Mainzer et al. 2014](#)).

When *WISE* was in its cryogenic phase, the focal planes operated at temperatures of 30-34 K for the W1 and W2 bands and ~ 7.8 K for the W3 and W4 bands ([Wright et al. 2010](#)). *NEOWISE* continued operating at the new equilibrium temperature of ~ 74 K, allowing the use of the W1 and W2 bands for all future observations. The W2 band spans strong gas emission lines from CO and CO₂ and so can be used to detect these species from space. Because W2 spans both CO and CO₂ emission lines (denoted as CO+CO₂), the two species cannot be differentiated by the *WISE/NEOWISE* photometry alone. Therefore we use Q_{CO_2} as a proxy for the production of both species, since the emission line of CO₂ is ~ 11.6 times stronger than the CO line ([Crovisier & Encrenaz 1983](#); [Bauer et al. 2015](#)). From this point forward the production rate of CO+CO₂ (units kg/s) from comets will be referred to as Q_{CO_2} .

2. OBSERVATIONS

The *WISE* spacecraft captures images every 11s with the active bands operating in unison and observing the same field of view using a beamsplitter ([Wright et al. 2010](#)). The telescope orbits Earth in a pole to pole orbit

near terminator and advances on the sky 1deg per day achieving full sky coverage roughly once every 6 months. This yields an average of ~ 12 exposures spaced over ~ 36 hours for most comets in the survey (Mainzer et al. 2011b; Cutri et al. 2012). The spacecraft may later detect the comet at a different part of its orbit. As in Bauer et al. (2015), all comet observations with multiple sets of detections within a given date range are referred to as epochs. The separation time between any two epochs is a minimum of ~ 3 days. The epochs are numbered in the order of which the comets were observed by the telescope. For example, if there are three different observations of the same comet, each observation will be chronologically labeled epoch 1, 2, and 3. If an observation is not included due to either clear comet inactivity or low SNR, the epoch is skipped. Each band (W1, W2, W3, and W4) has a different spatial resolution, 6.1, 6.4, 6.5, and 12.0 arcseconds, respectively, given as the FWHM of the mean point spread function (Wright et al. 2010; Cutri et al. 2012). The images we used were limited to detections of the comet with signal to noise ratios (SNR) ≥ 2.5 . All images used in this study were stacked single-exposure images produced by the WISE data pipeline. Of the objects used in this study, 10 have images gathered from the reactivated mission, while 5 objects have images gathered from the prime mission. All comet orbital properties can be found in Table 1, including the breakdown of objects with multiple visits. The date given for each epoch is the median time stamp of the stacked exposures in units of Modified Julian Date (MJD).

2.1. CO+CO₂ Producing HTC's

When all four bands of *WISE* were operational, reflected light emission was determined from the W1 fluxes, while thermal emission of dust was detectable in the W3 and W4 bands. The W2 ($4.6 \pm 0.5 \mu\text{m}$) band is most useful for detecting gas production rates because CO and CO₂ emit strong spectral lines at $4.67 \mu\text{m}$ and $4.23 \mu\text{m}$ respectively (Pittichová et al. 2008; Bauer et al. 2011; Reach et al. 2013). The spectral line emissions are strong enough to manifest as excess flux in the W2 band, relative to the signal level fit of reflected light and thermal emission present in the W1, W3, and W4 bands, thereby providing a metric for detection. Our sample does not consist of HTC's from the 3-band mission. However, there are 5 objects from the prime mission with measurements made in all four bands (27P, P/2006 HR30, P/2010 JC81, C/2010 L5, P/2012 NJ). To account for observations made by *NEOWISE*, a method was developed and applied in order to predict the thermal emission curve that was constrained by the

signals from the W3 and W4 bands during the prime mission (see Section 3.2).

3. ANALYSIS

In the reactivated *NEOWISE* Year I and Year II data, certain HTC's were identified as potential candidates for CO+CO₂ production by the following method. The images were stacked and photometrically analyzed in the same manner as described in Bauer et al. (2015). The *WISE* image data were processed using the scan and frame pipeline responsible for applying instrumental, photometric, and astronomical calibrations described in Section IV of Cutri et al. 2012. Initial data products were co-added using the software suite known as “A *WISE* Astronomical Image Co-Adder” (AWAIC) that takes advantage of advanced interpolation methods in order to maximize SNR (Masci & Fowler 2009). Emission flux was obtained by converting from signal count using the magnitude zeropoints corresponding to each W-band and 0th magnitude flux values procured from Wright et al. (2010). Color corrections and aperture photometry were performed on the stacked images with an 11 arcsecond radius. To assure that a stacked image contained a comet, and not a star or noise, we completed by-eye visual inspections of the selected HTC's with SNRs $\geq \sim 2.5$. At the completion of visual assessment, it was found that we had 11 candidates from the reactivated mission. Images of the HTC's 27P, P/2006 HR30, and P/2012 NJ from the prime mission were also used in this study for completeness. In addition, two epochs of C/2010 L5, and a single epoch of P/2010 JC81 were included from Bauer et al. (2015).

3.1. Nucleus Size

The methods used to determine nucleus size were similar to those described for comets in Bauer et al. (2015), and those described for asteroids in Masiero et al. (2012), Nugent et al. (2015), and Nugent et al. (2016). The diameter of the comets 27P, P/2006 HR30, P/2012 NJ, and C/2016 S1 were calculated using aspects of the Near-Earth Asteroid Thermal Model (NEATM) first described in Harris (1998). The model assumes a spherical object, with no rotation, no night side emission, and a temperature distribution given by Equation 1.

$$T(\theta) = T_{max} \cos^{1/4}(\theta) \text{ for } 0 \leq \theta \leq \pi/2 \quad (1)$$

For the above equation, θ is the angular distance from the sub-solar point and T_{max} can be defined as the sub-solar temperature given by Equation 2, in which S is defined as the solar flux at the asteroid, η is the beaming parameter as described in Harris (1998), A is the

Table 1. Orbital Properties of HTC^a

Object	i	e	q	Phase Ang	Image Stack Mid-point
	(deg)		(AU)	(deg)	(MJD)
27P (Crommelin)	28.97	0.9190	0.748	10.8	56719.2097
P/2006 HR30 (Siding Spring)	31.88	0.8431	1.226	6.40	55233.4654
P/2010 JC81 ^b	38.69	0.7773	1.811	15.0	55327.4473
C/2010 L5 Epoch 1 ^b	147.1	0.9037	0.791	57.5	55361.4543
C/2010 L5 Epoch 2 ^b	147.1	0.9037	0.791	39.0	55393.9793
P/2012 NJ (La Sagra) ^c	8.503	0.8481	1.292	8.10	55311.2952
C/2014 J1 (Catalina) Epoch 2	159.7	0.8023	1.709	36.4	56821.8230
C/2014 Q3 (Borisov) Epoch 2	89.95	0.9421	1.647	35.0	56936.2784
C/2014 Q3 Epoch 3	89.95	0.9421	1.647	36.7	56989.2271
C/2014 W9 Epoch 2	10.63	0.8578	1.587	37.6	57046.2495
C/2014 W9 Epoch 3	10.63	0.8578	1.587	38.0	57064.9394
C/2015 A1	80.37	0.9008	1.996	29.8	57085.1842
C/2015 GX Epoch 3	90.25	0.8782	1.972	22.0	57100.8549
C/2015 GX Epoch 4	90.25	0.8782	1.972	26.4	57157.8278
C/2015 GX Epoch 5	90.25	0.8782	1.972	29.4	57305.0489
C/2015 H1 (Bressi) Epoch 4	140.7	0.9408	1.926	30.2	57156.7226
C/2015 H1 Epoch 5	140.7	0.9408	1.926	24.9	57231.7971
C/2015 X8 Epoch 1	155.3	0.9393	1.190	43.6	57370.8975
C/2015 X8 Epoch 2	155.3	0.9393	1.190	30.1	57422.6712
C/2015 YG1	57.34	0.8792	2.073	25.9	57374.5027
C/2016 S1	94.69	0.7089	2.412	22.2	57723.6497

NOTE— ^a Orbital properties from objects observed during the reactivated phase of the mission except objects from (Bauer et al. 2015). The orbital parameters and phase angles were provided JPL’s HORIZONS ephemeris service; <https://ssd.jpl.nasa.gov/>. The orbital properties include orbital inclination (i), orbital eccentricity (e), and perihelion distance (q). The Image Stack Mid-Point in MJD was determined by finding the median stacked image date, except for objects provided by Bauer et al. (2015).

^b Orbital properties are from Bauer et al. (2015); these data are objects observed during the prime phase of the mission.

^c P/2012 NJ was not included in Bauer et al. (2015), but was observed during the cryogenic mission.

bolometric Bond albedo, ϵ is the emissivity, and σ is the Stefan-Boltzmann constant.

$$T_{max} = \left(\frac{(1 - A)S}{\eta \epsilon \sigma} \right)^{1/4} \quad (2)$$

NEATM was applied to our comets under the assumption that the coma was inactive and the object appeared point-like. We made this assumption due to the surface brightness profile of the comet matching that of a point spread function for *WISE*. For any given object we only have thermal data from the W2 band, thus any aberration between NEATM and the actual comet is accounted for using the beaming parameter η (Masiero et al. 2012). Such aberrations comprise of non-spherical shapes, variations in surface roughness or thermal inertia, the presence of satellites, uncertainties in emissivity, high rates

of spin, changes in surface temperature distributions due to spin pole location, or the imprecise assumption that the objects night-side has zero thermal emission (Nugent et al. 2015); for example $\eta = \pi$ is representative of a spherical body with high thermal inertia (Harris 1998). When generating the thermal profile, a crucial step in determining the albedo and diameter of the comet, η can be used to modify the temperature distribution of the model to account for any of these anomalies. For our analysis the beaming parameters were fixed if only one detection band had an acceptable SNR or if there was a detection in only the W1 band or the W2 band. In every other case η was left a free parameter and ranged from 0.63 to 1.3.

3.2. Dust Photometry and CO+CO₂ Production Measurements

Table 2. Dust and W2 Excess Analysis Results

Object	R _h	Delta	Q _{CO₂}	Afρ	CO ₂ /Afρ	Q _{CO₂} 3σ Upper
	AU	AU	molecules/cm	cm	molecules/cm·s	molecules/s
27P (Crommelin)	5.39	5.31				26.3
P/2006 HR30 (Siding Spring)	8.81	8.77				26.8
P/2010 JC81	3.90	3.76				25.5
C/2010 L5 Epoch 1	1.21	0.65	26.71 ± 0.25	1.95 ± 0.010	24.38 ± 0.25	
C/2010 L5 Epoch 2.	1.62	1.15	25.08 ± 0.08	2.64 ± 0.14	22.44 ± 0.16	
P/2012 NJ (La Sagra)	7.08	6.94				26.6
C/2014 J1 (Catalina) Epoch 2	1.71	1.35	25.18 ± 0.12	0.790 ± 0.036	24.39 ± 0.13	
C/2014 Q3 (Borisov) Epoch 2	1.74	1.40	26.71 ± 0.12	2.57 ± 0.010	24.13 ± 0.12	
C/2014 Q3 Epoch 3	1.65	1.32		2.56 ± 0.010		26.8
C/2014 W9 Epoch 2	1.61	1.26		1.57 ± 0.050		26.1
C/2014 W9 Epoch 3	1.59	1.12	26.16 ± 0.11	1.69 ± 0.011	24.47 ± 0.11	
C/2015 A1	2.00	1.73		1.51 ± 0.010		25.8
C/2015 GX Epoch 3	2.66	2.46	25.54 ± 0.12	1.31 ± 0.090	24.24 ± 0.15	
C/2015 GX Epoch 4	2.29	2.05	25.81 ± 0.10	1.30 ± 0.046	24.51 ± 0.11	
C/2015 GX Epoch 5	2.04	1.77	26.40 ± 0.10	1.98 ± 0.096	24.41 ± 0.14	
C/2015 H1 (Bressi) Epoch 4	2.01	1.72	25.83 ± 0.12	1.73 ± 0.031	24.10 ± 0.12	
C/2015 H1 Epoch 5	2.40	2.09	25.58 ± 0.12	1.59 ± 0.040	23.99 ± 0.13	
C/2015 X8 Epoch 1	1.43	1.03	26.00 ± 0.10	1.81 ± 0.056	24.19 ± 0.11	
C/2015 X8 Epoch 2	1.92	1.47	25.76 ± 0.12	1.56 ± 0.057	24.20 ± 0.13	
C/2015 YG1	2.26	2.04	26.24 ± 0.12	1.86 ± 0.15	24.38 ± 0.19	
C/2016 S1	2.60	2.34				25.5

NOTE—R_h is the comet-sun distance; Delta is the comet-Earth distance.

The quantity $Af\rho$, as determined in [Bauer et al. \(2015\)](#) and defined in [A' Hearn et al. \(1984\)](#), was calculated as a benchmark to compare comets within the HTC population. The quantity is calculated from the reflected light component of emission, presumably from the dust coma of the comets. $Af\rho$ consists of the albedo A , the filling factor f , and the aperture radius projected out to the distance of the comet ρ ([A' Hearn et al. 1984](#)). The filling factor is $f = N_g\sigma/\pi\rho^2$ with N_g being the number of dust grains in a given aperture and σ being the grain cross section.

$Af\rho$ can also be defined in the form of Equation 3, in which F_{comet} is the observed flux from the comet, F_{\odot} is the flux from the Sun evaluated at 1 AU, r is the Sun-comet distance in AU, and Δ is the Earth-comet distance in the same units as ρ (for ground-based observations), or in this case the distance between the comet and *NEOWISE* in the same units as ρ . The flux from the comet per unit area can also be thought of as $F/4\pi\Delta^2$, with F being the total cometary flux. The data pro-

vided by the W1 band were used to calculate $Af\rho$. $Af\rho$ is not independent of phase angle, and is known to affect dust production calculations ([A' Hearn et al. 1995](#)). To account for phase angle, a correction was made using the phase function as defined by [Agarwal et al. \(2007\)](#). The computation of $Af\rho$ is a necessary step in calculating Q_{CO_2} .

$$Af\rho = \frac{F_{\text{comet}}}{F_{\odot}} \frac{(2r\Delta)^2}{\rho} \quad (3)$$

The production rate of CO+CO₂ was calculated for objects observed during the prime mission from the excess signal ($\sim 3\sigma$) in the W2 band relative to the extrapolated thermal and reflected light contributions. The thermal contribution was determined by fitting a Planck function for an appropriate temperature to the W3 and W4 fluxes. Detections for our objects in the W3 and W4 bands were absent for the post-cryo and reactivation mission phases. Thus, the theoretical thermal emission curve was determined by calculating the expected black-

body radiation emission given the estimated amount of dust from the W1 flux. Assuming that dust grains both reflect light and emit thermally, we used the number of dust grains N_g to find a number surface density. Given the number density, a Planck function was generated using an infrared emissivity of ~ 0.9 , assuming a dust grain albedo near ~ 0.1 and assuming a blackbody temperature of $286\text{K} \times r_H^{-1/2}$ in which r_H (AU) is the heliocentric distance (Stevenson et al. 2015).

For each object, a plot of the detected reflected light flux (assumed to be a solar spectrum shape) and the estimated thermal signal was produced. The reflected light curve was constrained by detections in the W1 band. If there was excess flux detected by W2, such as in Figure 1, we assumed that this was due to Q_{CO_2} . This simplification was necessary due to the single data point from the reflected emission at $3.4 \mu\text{m}$ and due to the absence of longer wavelength data. The excess W2 signal flux, is converted to an average column density $\langle N \rangle$ in units of cm^{-2} by way of Equation 4.

$$\langle N \rangle = F_{\text{W}_2} 4\pi \Delta^2 \frac{\lambda}{hc} \frac{r^2}{g} \frac{1}{\pi \rho^2} \quad (4)$$

The variables present from Equation 3 share the same definition, F_{W_2} is the total W2 excess flux in units of $\text{erg s}^{-1} \text{cm}^2$, λ is the wavelength of the observation in units of μm , h is the Planck constant in units of erg s , c is the speed of light in units of μm , and $g = 2.86 \times 10^{-3} \text{s}^{-1}$ is the fluorescence efficiency for CO_2 at 1 AU (Crovisier & Encrenaz 1983). We calculate F_{W_2} after eliminating the inband nucleus dust signal contributions and integrating the resultant flux density over the CO/CO_2 bandpass.

Knowing $\langle N \rangle$ we can calculate Q_{CO_2} by Equation 5, where v is the gas ejection velocity assumed to be 0.62km s^{-1} consistent with Bauer et al. (2011), and 10^5 is a unit conversion factor. In order to calculate uncertainties for Q_{CO_2} we accounted for both the uncertainty from the photometry, and the uncertainty in the thermal emission calculation; both were added in quadrature.

$$Q_{\text{CO}_2} = \langle N \rangle 2\rho v \times 10^5 \quad (5)$$

In some cases only an upper limit of Q_{CO_2} could be calculated for the objects. We found this value by assuming that the comet was active and dominated by the dust emission signal. Furthermore, we found the value 1σ above and below the W2 band signal and considered the amount of CO_2 that would be produced given the blackbody estimate and given the scattered reflected light across the solar spectrum. If the 1σ photometric uncertainty fell on the curve created from the sum of the thermal emission curve and reflected light curve at W2, we calculated an upper limit. The combined pho-

tometry of the upper 1σ uncertainty and the W2 band signal was then used to find the 1σ Q_{CO_2} upper limit. For the purposes of our study, the 1σ upper limits were converted to 3σ upper limits.

When calculating either Q_{CO_2} or Q_{CO_2} upper limits we convert all excess flux into equivalent CO_2 production rates. However, if the excess is attributed solely to the production of CO , the equivalent CO production rates can be obtained by multiplying Q_{CO_2} by a factor of ~ 11.6 . Note that if CO is the dominant source of the emission, a mix of the two is very possible (cf. Fougere et al. 2016). Overall, the process to calculate Q_{CO_2} builds upon methods introduced by Pittichová et al. (2008) and is very similar to that developed in Bauer et al. (2011, 2012a,b, 2015); Stevenson et al. (2015).

C/2010 L5 Epoch 2 was not considered for this analysis due to its low $Af\rho$ value and further considerations from (Kramer et al. 2017) that indicate the comet underwent a single pathological outburst event without continuing activity in Epoch 2.

It was found that significant Q_{CO_2} signal (3σ) was found in all 11 of the reactivated mission's HTC's, shown in Table 3. We have a total of 13 measurements of Q_{CO_2} when including the two epochs of C/2010 L5 (Bauer et al. 2015). There were 8 other HTC's that demonstrated limited to no activity. However, we were able to calculate 3σ upper limits for Q_{CO_2} for each comet because the surface brightness profile matched the stellar point-spread function within the limits of uncertainty.

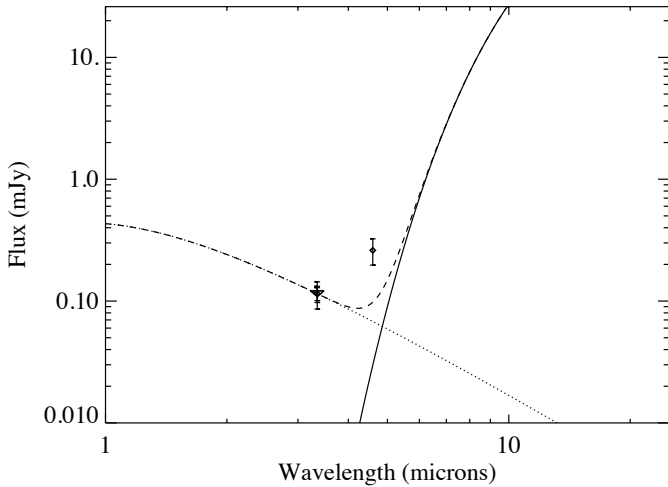


Figure 1. Example of 4.6 μm excess in the thermal signal for C/2015 H1 Epoch 2. The reflected light emission flux as a function of wavelength is represented by the dotted line and is constrained by data in the W1 band. The thermal emission flux as a function of wavelength is represented by the solid line and is approximated from data in the W1 band. The combined reflected light emission and thermal emission curve is represented by the dashed line. Note the 4.6 μm excess in combined reflected and thermal emission flux detected in the W2 band (\blacklozenge). Note that flux distributions are not shown for the comets 27P, P/2006 HR30, P/2012 NJ, and C/2016 S1, which appeared to be inactive, i.e. did not exhibit detectable coma, during the time of the NEOWISE observations. Flux distributions for C/2010 L5 can be found in [Kramer et al. 2017](#). The complete set of plots is available in the online journal.

4. DISCUSSION

4.1. Nucleus Size

The comet diameters in Table 3 provide a representation of the sizes of comets used in this study. The range in diameters is similar to those of long period comets. Due to concerns with the degree of activity of C/2016 S1 we calculated a 3σ upper limit diameter of 14 km. However, if our observation of C/2016 S1 was during a period of inactivity, we derived the diameter of the comet to be 5.2 ± 3 km. C/2010 L5 also has a calculated 3σ upper limit of 2.2 km ([Kramer et al. 2017](#)). It should be noted that the nucleus size of C/2010 L5 is much smaller than that of the other HTCs. In general, the nucleus mean diameter of the HTCs in this sample are on the order of Halley's effective diameter of 11 km ([Lamy et al. 2004](#)).

Table 3. HTC Nuclei Diameters^a

Object	Diam (km)	η
27P	12 ± 3	1.0, <i>fixed</i>
P/2006 HR30	16 ± 2	0.63 ± 0.1
C/2010 L5 ^a	≤ 2.2	—
P/2012 NJ	19 ± 2	1.3 ± 0.2
C/2016 S1	5.2 ± 3	1.0, <i>fixed</i>

NOTE— ^a η is the beaming parameter.

^b Diameter from [Kramer et al. \(2017\)](#).

4.2. Dust Production Rates and CO+CO₂ Production Rates

In order to examine the relationship between our independent variables ($Af\rho$, Q_{CO_2} , $Q_{\text{CO}_2}/Af\rho$) and R_h , we calculated both the Spearman rank correlation coefficient (ρ_s) and the Kendall- τ (τ). The strength and direction of the monotonic relationship between two continuous or ordinal variables is described by ρ_s , and can range from -1 to 1 . A value of -1 indicates a perfect negative correlation and 1 indicates a perfect positive correlation, a value of 0 indicates no correlation between variables. The significance of ρ_s was found by calculating the two-tailed p -value. A p -value for ρ_s can range from 0 to 1 , the closer the value is to 0 , the greater the significance of the result. It should be noted that the p -value calculated for a given ρ_s may not be reliable for a sample of our size, thus a τ test was also implemented to our data. The main difference between τ and ρ_s is that the calculations for τ are based on concordant and discordant pairs in the data, and the calculations for ρ_s are based on deviations in the data. This fact makes the τ test more accurate for smaller sample sizes. Like ρ_s , τ can range from -1 to 1 ; a value of -1 indicating a negatively correlated pair, 0 indicating no correlation, and 1 indicating a positively correlated pair. Again, the significance of the test was determined by calculating a two-tailed p -value. Originally, polynomial fits of the data were attempted; however, our sample size was too small and our error too large to meaningfully constrain or identify any power law relationship.

The relationship between R_h from 1.21 to 2.66 AU and dust production rates of the HTCs is shown in Figure 2. Comets with a lower $Af\rho$ can be thought of as relatively dust poor or inactive. The rank correlation tests returned a value of $\rho_s = -0.32$ with a p -value = 0.25 , and a value of $\tau = -0.24$ with a p -value = 0.22 , indicating that there is little to no significant correlation between $Af\rho$ and R_h within 1.21 and 2.66 AU.

The relationship between Q_{CO_2} and R_h can be found in Figure 3. The statistics only consider known Q_{CO_2} values and not the calculated 3σ upper limits. The rank correlation tests for Q_{CO_2} returned a value of $\rho_s = -0.42$ with a p -value = 0.17 and a value of $\tau = -0.33$ with a p -value = 0.13.

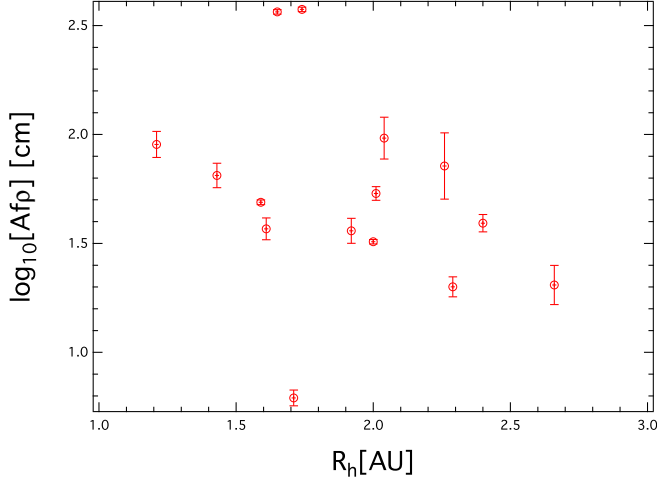


Figure 2. Plot of $Af\rho$ with respect to R_{Helio} derived from $3.4\ \mu\text{m}$ flux for active HTC's.

Again, this indicates that there is little to no significant correlation between Q_{CO_2} and R_h for the sample range. For the upper limit of CO_2 production rates for C/2014 Q3, C/2014 W9, and C/2015 A1 it should be noted that R_h was at or under 2 AU. For this reason, it is clear from the flux plots in the Appendix that the W2 flux is ever so slightly higher than the thermal curve, but still within the limits of the combined 3σ uncertainty of the photometry and the model. Due to the proximity to the Sun, the W2 band may have a more significant thermal signal relative to the reflected light signal, leading to a non-optimal prediction of the Planck function. As previously mentioned, the thermal curves are predictions modeled with assumptions from the W1 band data because of the unavailability of the W3 and W4 band data. For this reason there could be a more significant thermal component than the assumed model would suggest. Due to the relatively large heliocentric distances of 27P, P/2006 HR30, C/2010 JC81, and P/2012 NJ, the respective upper limits were not significant and fell outside the plotted range of R_h in Figure 3. At these distances the activity of the comet could be considered minimal.

To consider the nature of dust production and Q_{CO_2} with respect to R_h , we plotted the ratio of Q_{CO_2} to $Af\rho$ in Figure 4. Our aspiration was to observe if this value indicated any consistency across the HTC's

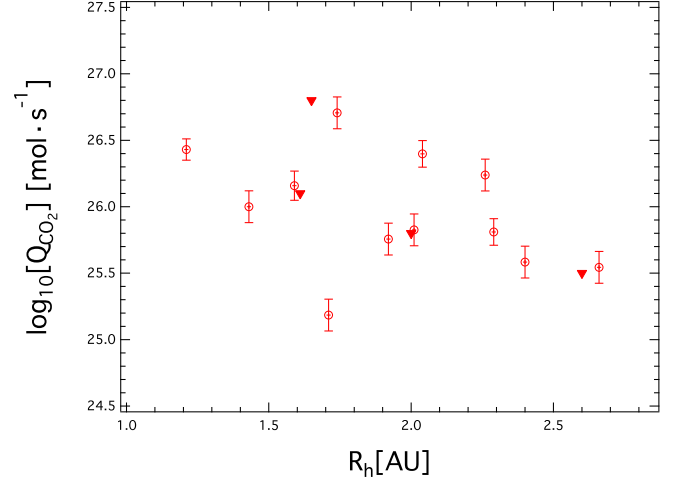


Figure 3. Plot of Q_{CO_2} of HTC's (red circles) with respect to heliocentric distance with Q_{CO_2} upper limits (\blacktriangledown) included.

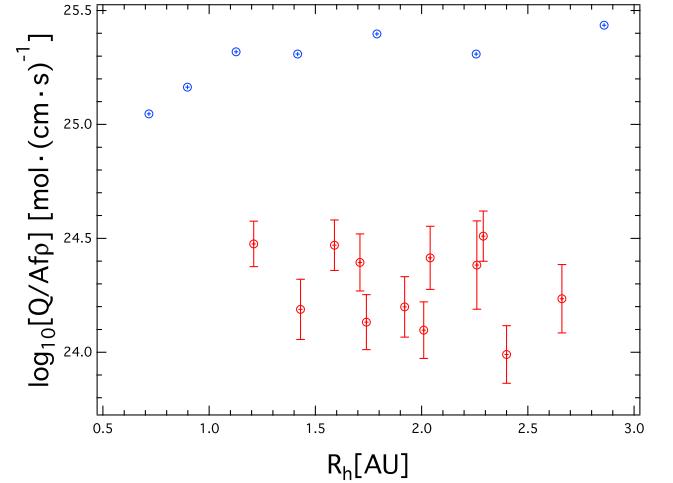


Figure 4. Plot of $\log_{10} Q_{\text{CO}_2}/Af\rho$ (red circles) as a function of the heliocentric distance. The points in blue are $Q_{\text{OH}}/Af\rho$ with respect to heliocentric distance of 1P Halley as presented by A'Hearn et al. (1995).

for gas to dust ratios. Again, we note that after completing the rank correlations for $Q_{\text{CO}_2}/Af\rho$, we find $\rho_s = -0.20$ with a p -value = 0.53, and $\tau = -0.18$ with a p -value = 0.41, indicating that there is little to no correlation with heliocentric distance, but a rather consistent nature of gas to dust production across the objects. It is important to note that, when comparing the behavior of $Q_{\text{OH}}/Af\rho$ for comet 1P/Halley from A'Hearn et al. 1995, the slope of the line is relatively flat for the R_h range of our dataset. We can compare $Q_{\text{OH}}/Af\rho$ for comet Halley with $Q_{\text{CO}_2}/Af\rho$ for our comets to find that Q_{CO_2} is roughly $\sim 10\%$ on average of Q_{OH} for the same range in R_h . At these distances, then, it is perhaps not surprising that, as with

other comets, H₂O, the parent of OH, likely dominates activity. For all three cases, the lack of correlation to R_h would indicate that HTC's with $1.21 \leq R_h \leq 2.66$ AU have production values for both dust and CO+CO₂ that are independent of heliocentric distance.

5. CONCLUSIONS

The 11 HTC's analyzed in this study indicate the following:

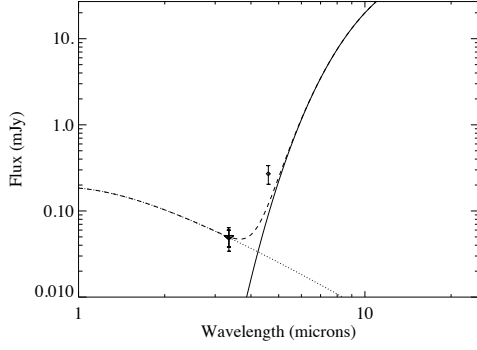
1. We find no significant correlation between heliocentric distance of 1.21 to 2.66 AU and $Af\rho$.
2. We also find no significant correlation between heliocentric distance of 1.21 to 2.66 AU and Q_{CO_2} .
3. We also find no significant correlation between heliocentric distance of 1.21 to 2.66 AU and $Q_{\text{CO}_2}/Af\rho$, consistent with $Q_{\text{OH}}/Af\rho$ for comet 1P, possibly implying that the rate of dust produced relative to the rate of CO+CO₂ produced is independent of the HTC's distance from the Sun.
4. The behavior observed for this sample of HTC's is not dissimilar from that of the LPCs observed in [Bauer et al. 2015](#) within 4 AU. However, the results from [Bauer et al. 2015](#) were primarily for $\epsilon f\rho$ which is an equivalent of $Af\rho$; the difference being $\epsilon f\rho$ is derived from reflected light emission rather than thermal emission.
5. The newly-derived diameters of HTC's nuclei shown in Table 3 are in the range of the ~ 11 km size found for 1P's nucleus from spacecraft encounters.

6. ACKNOWLEDGMENTS

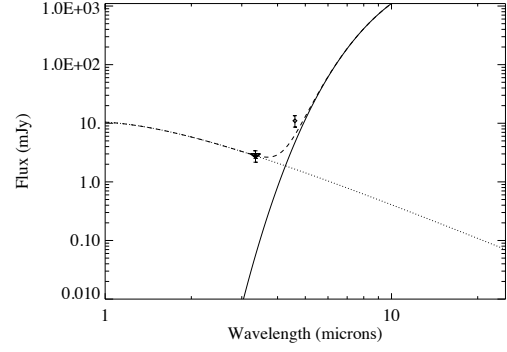
This research makes use of the data products from the *Wide-field Infrared Survey Explorer*, a joint venture between the University of California, Los Angeles, and the Jet Propulsion Laboratory/California Institute of Technology, funded by the National Aeronautics and Aerospace Administration. This paper also makes use of data products from *NEOWISE* a JPL/Caltech project, funded by the Planetary Science Division of NASA.

Software: Astropy ([Astropy Collaboration et al. 2013](#)), AWAIC ([Masci & Fowler 2009](#)), IDL ([Exelis Visual Information Solutions](#), Boulder, Colorado), Igor Pro ([WaveMetrics](#)), Python ([Python Software Foundation](#)), Pandas ([McKinney 2010](#)), Scipy ([Jones et al. 2001–](#); [Oliphant 2007](#); [Millman & Aivazis 2011](#))

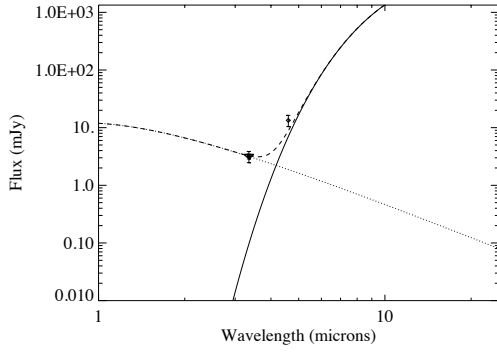
APPENDIX



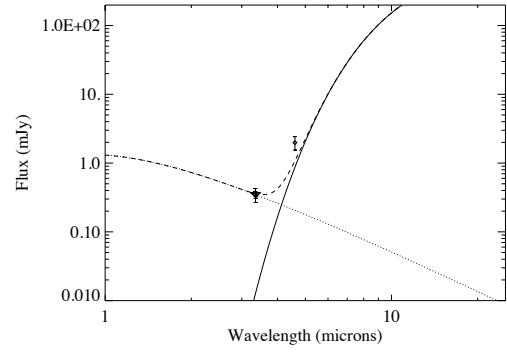
(c)



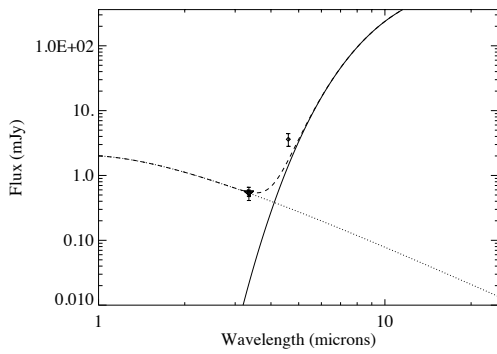
(d)



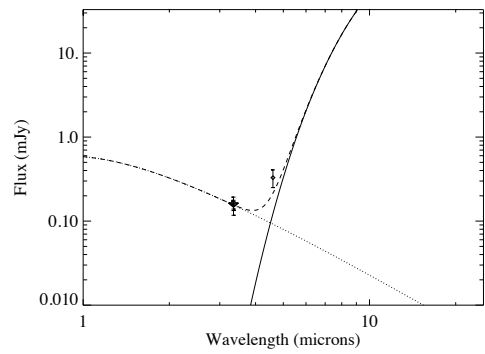
(e)



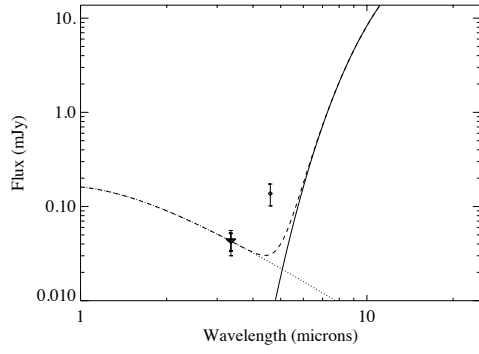
(f)



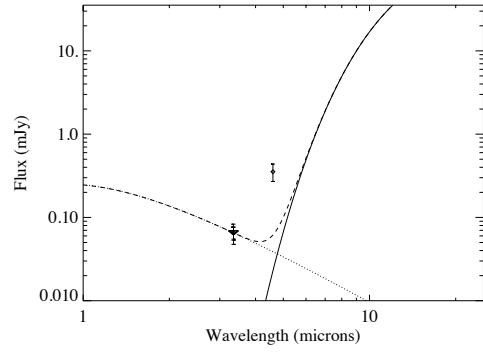
(g)



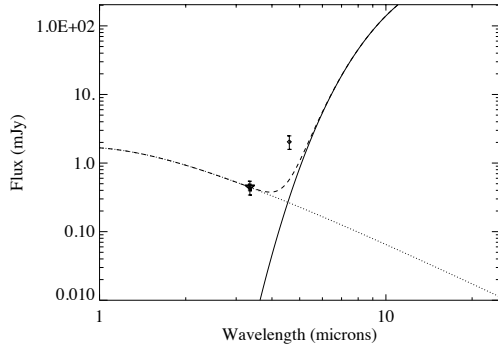
(h)



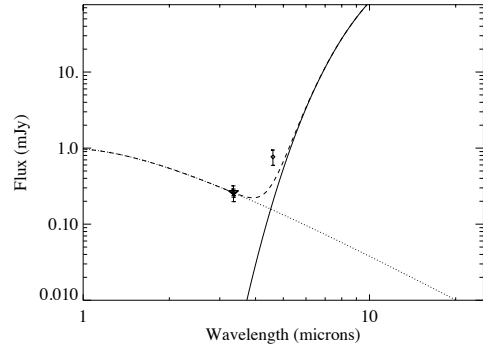
(i)



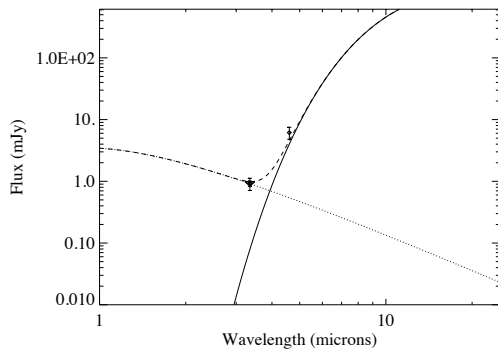
(j)



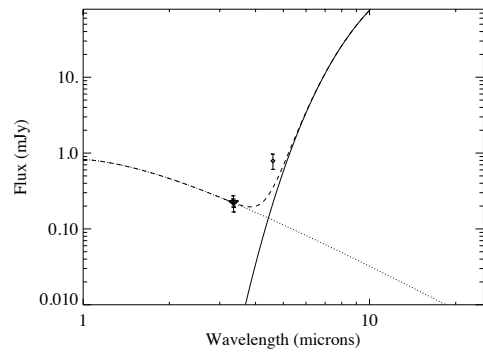
(k)



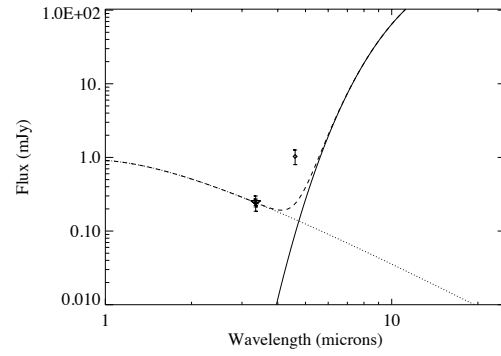
(l)



(m)



(n)



(o)

Figure 5. Model of dust spectral flux distribution and $4.6 \mu\text{m}$ excess for HTCs with significant W2 excess (See Figure 1). (a) C/2014 J1, (b) C/2014 Q3 Epoch 2, (c) C/2014 Q3 Epoch 3, (d) C/2014 W9 Epoch 2, (e) C/2014 W9 Epoch 3, (f) C/2015 A1, (g) C/2015 GX Epoch 3, (h) C/2015 GX Epoch 4, (i) C/2015 GX Epoch 5, (j) C/2015 H1 Epoch 4, (k) C/2015 X8 Epoch 1, (l) C/2015 X8 Epoch 2, (m) C/2015 YG1.

REFERENCES

- Agarwal, J., Müller, M., & Grün, E. 2007, *Space Science Reviews*, 128, 79.
<http://dx.doi.org/10.1007/s11214-006-9139-1>
- Astropy Collaboration, Robitaille, T. P., Tollerud, E. J., et al. 2013, *A&A*, 558, A33
- A'Hearn, M. F., & Dixi Science Team. 2011, in *Lunar and Planetary Inst. Technical Report*, Vol. 42, *Lunar and Planetary Science Conference*, 2516
- A'Hearn, M. F., Millis, R. C., Schleicher, D. O., Osip, D. J., & Birch, P. V. 1995, *Icarus*, 118, 223
- A' Hearn, M. F., Schleicher, D. G., Millis, R. L., Feldman, P. D., & Thompson, D. T. 1984, *The Astronomical Journal*, 89, 579. http://adsabs.harvard.edu/cgi-bin/bib_query?1984AJ.....89..579A
- Bauer, J. M., Walker, R. G., Mainzer, A. K., et al. 2011, *The Astrophysical Journal*, 738, 171.
<http://stacks.iop.org/0004-637X/738/i=2/a=171?key=crossref.e57c4b42bcadad16e88eaf4d94bef0b7>
- Bauer, J. M., Kramer, E., Mainzer, A. K., et al. 2012a, *The Astrophysical Journal*, 758, 18.
<http://stacks.iop.org/0004-637X/758/i=1/a=18?key=crossref.872f770455079892dfa36bbbe9020816>
- Bauer, J. M., Mainzer, A. K., Grav, T., et al. 2012b, *The Astrophysical Journal*, 747, 49.
<http://stacks.iop.org/0004-637X/747/i=1/a=49?key=crossref.3104da3d9439d86c872148018cb41a5c>
- Bauer, J. M., Grav, T., Erin, B., et al. 2013, *The Astrophysical Journal*, 773, 22.
<http://stacks.iop.org/0004-637X/773/i=1/a=22?key=crossref.7c50420568dd0a234767673dc4df1413>
- Bauer, J. M., Stevenson, R., Kramer, E., et al. 2015, *The Astrophysical Journal*, 814, 85.
<http://stacks.iop.org/0004-637X/814/i=2/a=85?key=crossref.24cad07842754e6352e39139d3d9402a>
- Bauer, J. M., Grav, T., Fernández, Y. R., et al. 2017, *AJ*, 154, 53
- Bönnhardt, H., Mumma, M. J., Villanueva, G. L., et al. 2008, *The Astrophysical Journal Letters*, 683, L71.
<http://stacks.iop.org/1538-4357/683/i=1/a=L71>
- Crovisier, J., & Encrenaz, T. 1983, *A&A*, 126, 170
- Cutri, R. M., et al. 2012, *Explanatory Supplement to the WISE All-sky Data Release*, . <http://wise2.ipac.caltech.edu/docs/release/allsky/expsup/>
- Dones, L., Brasser, R., Kaib, N., & Rickman, H. 2015, *SSRv*, 197, 191
- Fernández, Y. R., Kelley, M. S., Lamy, P. L., et al. 2013, *Icarus*, 226, 1138
- Fougere, N., Altwegg, K., Berthelier, J.-J., et al. 2016, *MNRAS*, 462, S156
- Harris, A. W. 1998, *Icarus*, 131, 291
- Jewitt, D. 2014, *Activity in Comets Beyond the Water Sublimation Zone*, *Keck Observatory Archive LRIS U072LA*, ,
- Jones, E., Oliphant, T., Peterson, P., et al. 2001–, *SciPy: Open source scientific tools for Python*, , [Online; accessed [today]]. <http://www.scipy.org/>
- Kramer, E., Bauer, J. M., B., Fernandez, Y. R., et al. 2017, *The Astrophysical Journal*, 128, 79.
<http://dx.doi.org/10.1007/s11214-006-9139-1>
- Lamy, P. L., Toth, I., Fernandez, Y. R., & Weaver, H. A. 2004, *The sizes, shapes, albedos, and colors of cometary nuclei*, ed. M. C. Festou, H. U. Keller, & H. A. Weaver, 223–264
- Licandro, J., Alí-Lagoa, V., Tancredi, G., & Fernández, Y. 2016, *A&A*, 585, A9
- Mainzer, A., Grav, T., Masiero, J., et al. 2011a, *The Astrophysical Journal Letters*, 737, L9.
<http://stacks.iop.org/2041-8205/737/i=1/a=L9>
- Mainzer, A., Bauer, J., Grav, T., et al. 2011b, *The Astrophysical Journal*, 731, 53.
<http://stacks.iop.org/0004-637X/731/i=1/a=53>
- Mainzer, A., Grav, T., Masiero, J., et al. 2012, *The Astrophysical Journal*, 752, 110.
<http://stacks.iop.org/0004-637X/752/i=2/a=110>
- Mainzer, A., Bauer, J., Cutri, R. M., et al. 2014, *The Astrophysical Journal*, 792, 30.
<http://stacks.iop.org/0004-637X/792/i=1/a=30>
- Masci, F. J., & Fowler, J. W. 2009, in *Astronomical Society of the Pacific Conference Series*, Vol. 411, *Astronomical Data Analysis Software and Systems XVIII*, ed. D. A. Bohlender, D. Durand, & P. Dowler, 67
- Masiero, J. R., Mainzer, A. K., Grav, T., et al. 2012, *The Astrophysical Journal Letters*, 759, L8.
<http://stacks.iop.org/2041-8205/759/i=1/a=L8>
- McKinney, W. 2010, in *Proceedings of the 9th Python in Science Conference*, ed. S. van der Walt & J. Millman, 51 – 56
- Meech, K. J., Hainaut, O. R., & Marsden, B. G. 2004, *Icarus*, 170, 463
- Meech, K. J., & Svoren, J. 2004, *Using cometary activity to trace the physical and chemical evolution of cometary nuclei*, ed. M. C. Festou, H. U. Keller, & H. A. Weaver, 317–335
- Millman, K. J., & Aivazis, M. 2011, *Computing in Science Engineering*, 13, 9
- Mumma, M. J., DiSanti, M. A., Bonev, B. P., et al. 2012, in *LPI Contributions*, Vol. 1667, *Asteroids, Comets, Meteors 2012*, 6199

- Nugent, C. R., Mainzer, A., Masiero, J., et al. 2015, ApJ, 814, 117
- Nugent, C. R., Mainzer, A., Bauer, J., et al. 2016, AJ, 152, 63
- Oliphant, T. E. 2007, Computing in Science Engineering, 9, 10
- Ootsubo, T., Usui, F., Kawakita, H., et al. 2010, ApJL, 717, L66
- Pittichová, J., Woodward, C. E., Kelley, M. S., & Reach, W. T. 2008, AJ, 136, 1127
- Reach, W. T., Kelley, M. S., & Vaubaillon, J. 2013, Icarus, 226, 777
- Stevenson, R., et al. 2015, ApJ
- Wiegert, P., & Tremaine, S. 1999, Icarus, 137, 84
- Wright, E. L., Eisenhardt, P. R. M., Mainzer, A. K., et al. 2010, The Astronomical Journal, 140, 1868.
<http://stacks.iop.org/1538-3881/140/i=6/a=1868?key=crossref.7bc383db470f437aa421907552685839>